



OPEN

A facile hydrothermal synthesis of high-efficient NiO nanocatalyst for preparation of 3,4-dihydropyrimidin-2(1H)-ones

Maryam Khashaei¹, Leila Kafi-Ahmadi^{1✉}, Shahin Khademinia², Ahmad Poursattar Marjani³ & Ehsan Nozad³

The present work introduces a one-step and facile hydrothermal procedure as a green process for the first time to synthesize nickel(II) oxide (NiO) nanoparticles. The as-prepared nanomaterials were used as high efficient, low toxic and cost catalyst for the synthesis of some organic compounds. Ni(NO₃)₂ and some natural extract were used as a surfactant for the first time to synthesis NiO nanomaterials. A high synthesis yield (91%) was obtained for S₂. Rietveld analysis affirmed the cubic crystal system of the obtained NiO nanocatalyst. The morphology studies were carried out with the FESEM method and the images revealed a change from non-homogenous to homogenous spherical particles when the Barberrys was used instead of orange blossom surfactant. Besides, the images revealed that the particle size distribution was in the range of 20 to 60 nm. The synthesized catalysts were used for the first time in Biginelli multicomponent reactions (MCRs) for the preparation of 3,4-dihydropyrimidin-2(1H)-ones (DHPMs) under the present facile reaction conditions. High yield (97%) of the final product was achieved at the optimum condensation reaction conditions (Catalyst: 60 mg; temperature: 90 °C and time: 90 min) when ethyl acetoacetate/methyl acetoacetate (1 mmol), benzaldehyde (1 mmol) and urea (1.2 mmol) were used. A kinetic study affirmed pseudo-first-order model for Biginelli reactions followed the pseudo-first-order model.

Researchers are intensely interested in the synthesis of nanomaterials due to their specific properties. The nanomaterials functions are strongly dependent on their shape and size, making these factors highly considerable for their applications¹. Nickel oxide (NiO) is a broad band gap antiferromagnetic p-type semiconductor². NiO nanoparticles are used in gas sensors³, batteries⁴, transparent conducting layers⁵, solar thermal absorbers⁶, electrochromic devices⁷, optical fibers⁸, smart windows⁹ and photocatalysts¹⁰.

It has been reported that NiO has the optical band gap of 2.3–3.5 eV^{11,12}. Various methods including coprecipitation¹¹, sol-gel¹², thermal decomposition¹³, microwave pyrolysis¹⁴, solvothermal¹⁵, anodic arc plasma¹⁶, sonochemical^{17,18}, microemulsion¹⁹, hydrothermal²⁰, solid-state²¹, boiling²² methods, green biosynthesis²³ and etc. have been reported for NiO synthesis. Green synthesis is a field of study aiming to design clean products and sustainable processes by reducing or even not using the unsafe solvents nor toxic reagents. In this respect, the green synthesis is potential for environmental sustainability promotion. In addition, ecofriendly synthesis reactions fulfill the green chemistry essentials that lead to preparation of low cost, straightforward, stable, and relatively reproducible nanomaterials^{24–30}.

Plant extracts, fungi, enzymes, and microorganisms are used as raw materials for green synthesis of nanoparticles. A plant-extract controlled nanoparticle synthesis has received a lot of attention due to its versatility^{31,32}.

Application of plant extracts as reducing, stabilizing, and capping agent accompanied by other notable features such as ease of use, cost effectiveness, and environmental friendliness make them highly valuable materials^{30,33}.

The capped nanoparticles can be prepared using plant extract phytochemicals as strong reducing agents that decrease the number of process steps, the cost and chemical use as a consequence^{31,32,34}.

In an aqueous system, phytocompounds are substituted with chemicals and organic/inorganic solvents³⁵. Extract of plant's different parts like flower, leaf, fruit and etc. are currently used to prepare nanoparticles^{32,36,37}.

¹Department of Inorganic Chemistry, Faculty of Chemistry, Urmia University, Urmia, Iran. ²Department of Inorganic Chemistry, Faculty of Chemistry, Semnan University, Semnan, Iran. ³Department of Organic Chemistry, Faculty of Chemistry, Urmia University, Urmia, Iran. ✉email: l.kafiahmadi@urmia.ac.ir

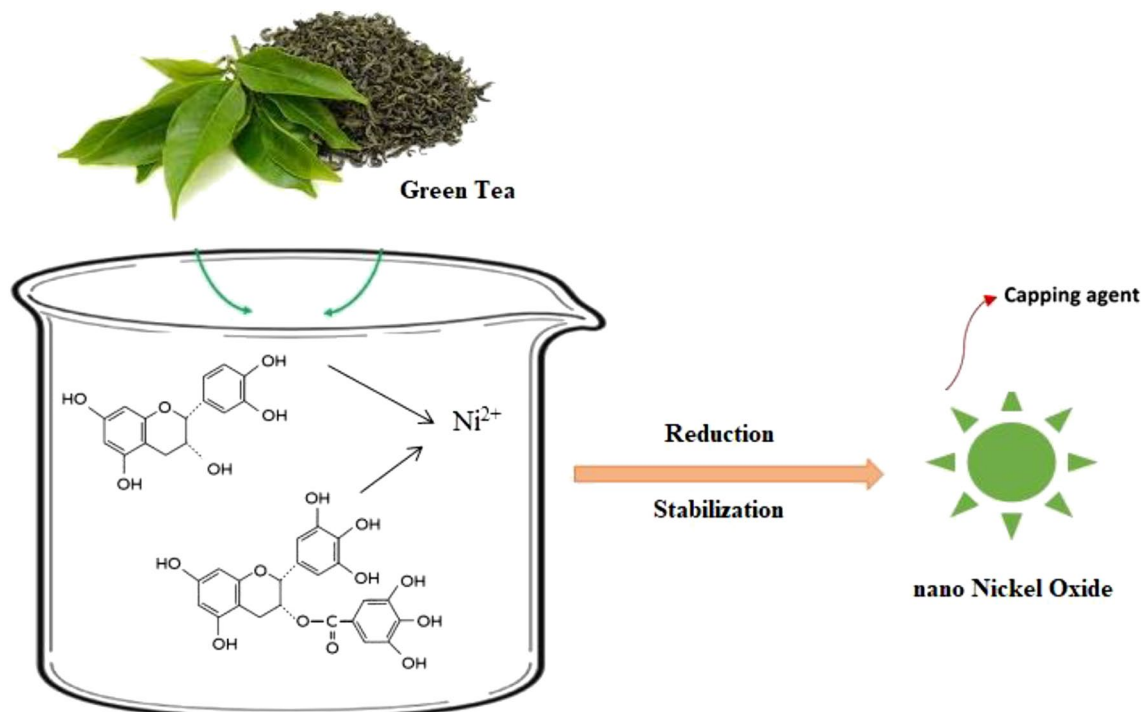


Figure 1. Schematic representation of the biosynthetic pathway of NiO nanoparticles using green tea extract for example.

The active biomolecules consist of amino, hydroxyl, carboxyl bifunctional groups, alkaloids, flavonoids, and terpenoids that would act as the reductant of metal salts and protective agents to form stabilizing layer on the biosynthesized nanoparticles (Fig. 1)^{23,25,26,29–32,38}.

Multicomponent reactions (MCRs) are some reactions that three or more reagents react in a one-pot process to form a new product. MCRs have obtained attentiveness in synthesis and medicinal chemistry in as much as the advantage of one-pot single reaction preparation of some strategic organic molecules and structures^{39,40}. Such reactions not only reduce the energy and solvent required but also lead to highly selective products. Owing to multiple benefits of MCRs process, the development of novel eco-friendly and NP-catalyzed MCRs procedures have been considered as an interesting growing field of research in organic chemistry^{27,28,41,42}.

Biginelli reaction is a procedure for the synthesis of 3,4-dihydropyrimidin-2(1H)-ones (DHPMs) in a one-step process. These compounds have wide biological antihypertensive, antiviral, antitumor, antibacterial, antioxidant and anti-inflammatory applications^{43,44}.

Several researches have confirmed the biological activities of DHPMs and their successful synthesis through Biginelli reactions via different metal oxides have been reported^{45–48}.

As part of our ongoing attempts in the field of catalysts^{48,49} to find a reusable high yield catalyst with low cost and toxicity, NiO nanocatalyst was synthesized by a novel and simple surfactant assisted mild condition hydrothermal procedure. Hibiscus tea, Orange blossom, Yarrow, Green tea, Barberries and Rosemary were used as natural surfactants in order to explore their effects on the growth of crystals, morphology and catalytic performance of NiO semiconductors. Rietveld analysis data were applied to investigate the extract effect on the experimental crystallographic properties of the prepared nanocatalyst. The optical properties and morphology of the materials were studied by UV–Vis spectroscopy and FE-SEM respectively. The high catalytic performance of the synthesized NiO nanomaterials was confirmed by their application as novel heterogeneous catalysts for the synthesis of DHPMs by Biginelli MCRs (Fig. 2). Besides, optimization of the factors (amount of catalyst, time and temperature of reaction) affecting the DHPMs synthesis process was evaluated by experimental design method. Therefore, synthesis of highly pure NiO nanoparticles by a new route and its application as a novel, low toxic, inexpensive, and high efficient catalyst to synthesize DHPMs is reported in this research for the first time.

Experimental

Materials and instruments. All precursors for the synthesis were purchased from Merck Co. (Germany) and no excess purification was carried out. Analytical grade of $\text{Ni}(\text{NO}_3)_2 \cdot 6\text{H}_2\text{O}$ and 25 V/V% NH_3 were prepared from Merck Co. The Hibiscus Sabdariffa L. Tea (Hibiscus tea), Citrus Sinensis (Orange blossom), Achillea Millefolium (Yarrow), Camellia Sinensis (Green tea), Barberis (Barberries) and Salvia Rosmarinus (Rosemary) were purchased from local market, Urmia, West Azerbaijan, Iran and all permissions were obtained for their application. The plants were then processed to obtain the desired extracts. X-ray Powder Diffraction (PXRD) patterns were recorded by a D5000 powder X-ray diffractometer (Siemens AG, Germany) using CuK α radiation to make phase identification. FullProf software was applied to accomplish the Rietveld analysis. Lattice parameter (a), $\sin\theta/\lambda$, FWHM (B(rad)), Bragg residual factor (R_{Bragg}), residual factor (RF), profile residual factor (Rp),

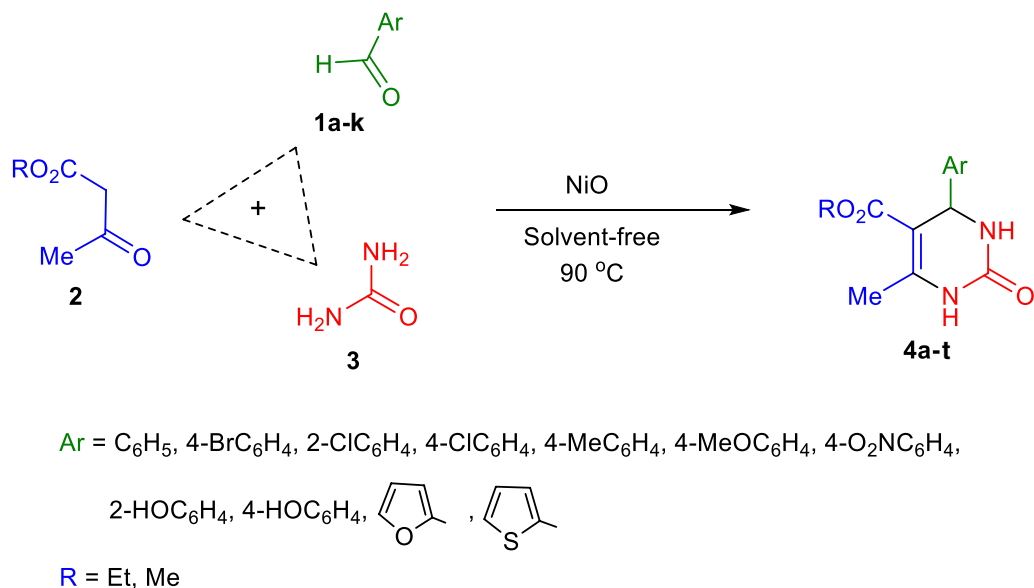


Figure 2. Schematic representation of the reaction pathway for the synthesis of DHPMs.

weighted profile residual factor (Rwp), expected residual factor (Rexp), the goodness of Rietveld refinement (χ^2), growth, purity values and crystal phase type, were investigated by Rietveld analysis. The FE-SEM images were taken on a Hitachi model S-4160 for morphologic studies. Absorption spectra were obtained with a UV-visible spectrophotometer (UV-1650 PC, Japan). A Tensor 27 FTIR spectrometer (Bruker, Germany) was used to obtain the spectra. Thin layer chromatography (TLC) using ethyl acetate/n-hexane mixture was used to evaluate the products purity. The melting points of the as-prepared DHPMs were measured using thermo scientific 9100 apparatus. ^1H NMR spectra were recorded by a Bruker Avance DRX-400 spectrometer (Bruker, Germany) using TMS as internal reference and in $\text{DMSO-}d_6$ as solvent.

Plant extraction process. All plants were dried and grounded to obtain a powder. 300 mg was poured in 30 mL of distilled water under agitation at raised temperature up to 70 °C for a short period. The final extracts then were cooled down following by filtration process and kept at a decreased temperature (4 °C) until next usage. This process was repeated for all plants.

All experimental protocols were performed in accordance with relevant institutional, national, and international guidelines and legislation.

Green synthesis of NiO nanomaterials. In a typical experiment, $\text{Ni}(\text{NO}_3)_2 \cdot 6\text{H}_2\text{O}$ (7 g) was dissolved in deionized water (50 mL). Then, after adding one of the natural surfactants (20 mL) [Orange blossom (S_1), Yarrow (S_2), Hibiscus tea (S_3), Green tea (S_4), Rosemary (S_5) and/or Barberry (S_6)], the pH was adjusted at 7 using a 25 V/V% ammonia solution and then stirred for 48 h on a magnetic stirrer. In the next step, the obtained solution was kept under ultra-sonication (30 min) and the final solution was poured into an autoclave, sealed and heated up to 80 °C for 24 h. Then, the reaction container was cooled down by water immediately and the synthesized nanocatalyst was washed with distilled water and dried at 115 °C for 2 h. To obtain the final product, the nanocatalyst was treated in an electrical furnace at 410 °C for 10 h to remove the residual organic components and a gray-black powder was obtained.

Synthesis of DHPMs. A mixture of arylaldehyde (1 mmol), ethyl acetoacetate/methyl acetoacetate (1 mmol), urea (1.2 mmol) and 30 mg (0.04 mol%) of the nanocatalyst were mixed and stirred. Biginelli reaction parameters were optimized with design expert software. After reaction completion, the final solid crude product was rinsed with deionized water to remove the unreacted materials. The catalyst was separated from the precipitated solid by dissolving the compound in ethanol. Then, the filtrated solution was left undisturbed to obtain the pure product crystals. In the experimental design of the reactions, the effective parameters were changed simultaneously until an optimum condition was obtained to find out the best reaction yield. The yield of each reaction was determined with mmol fraction measurement of the considered DHPMs. The spectra data of the prepared compounds are provided in supporting information.

Results and discussions

Characterization. *X-ray diffraction analysis.* The as-synthesized NiO samples were characterized by XRPD patterns (Fig. 3). To study the structural properties of the synthesized nanomaterials, the XRD data were analyzed by *FullProf* program. In the Rietveld analysis accomplished by the *FullProf* program, the observed and calculated data are shown in red and black lines respectively that are obtained with the Rietveld refinement. The blue line is the difference: $\text{Yobs} - \text{Ycalc}$. The patterns indicate a pure NiO cubic crystal structure with Fm-3 m

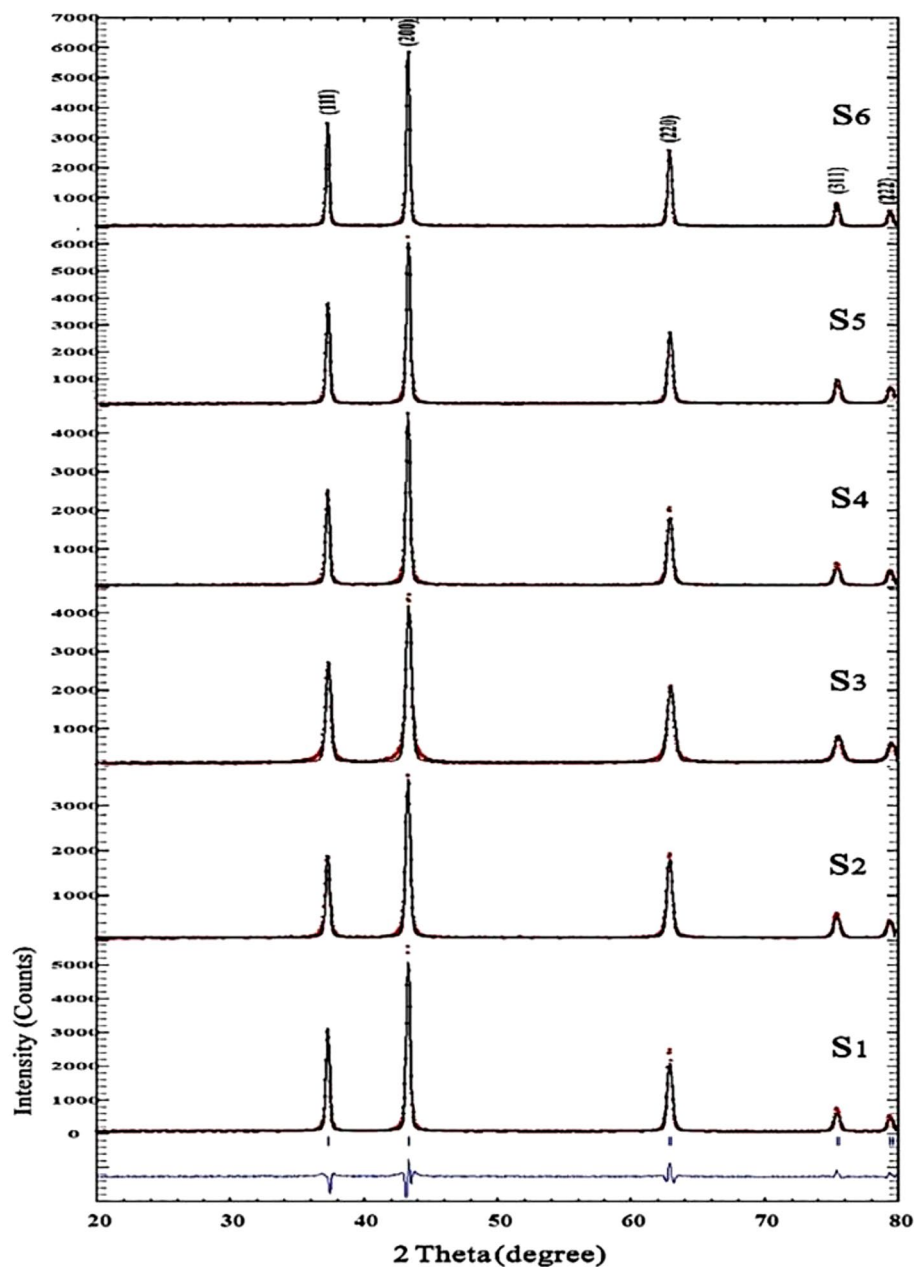


Figure 3. PXRD patterns of the NiO nanomaterials synthesized by hydrothermal method at 80 °C for 24 h followed by a calcination at 400 °C for 10 h refined by the Rietveld analysis.

space group for S_1 to S_6 nanocatalysts²⁻⁶. The peaks positions emerging at $2\theta = 37.23^\circ$, 43.26° , 62.83° , 75.36° and 79.35° are indexed to (111), (200), (220), (311), and (222) crystal planes of the as-synthesized NiO nanomaterials, respectively. The above-mentioned characteristic diffraction peaks can be perfectly indexed to the face-centered cubic (FCC) crystalline structure in view of their peak position and relative intensity. It can be observed that the samples are single phase and no peak related to impurity was observed except the characteristic peaks of FCC phase. According to Table 1, changing the surfactant type has no considerable effect on the unit cell volume of the targets. However, it was found that the crystal phase growth is varied by changing the surfactant type. The lowest and highest crystal phase growth is achieved when Yarrow and Barberrry surfactants are used respectively.

Some crystallographic parameters such as crystallite size (D), strain (ϵ), interplanar spacing (d), dislocation density (δ), and X-ray density (D_x) were calculated and tabulated in Table 2. The crystallite size data were calculated by Scherrer equation:

$$D = \frac{K\lambda}{B_{\frac{1}{2}} \cos \theta} \quad (1)$$

Entry	Sample	a	V	R _F	R _B	χ ²	R _p	R _{wp}	R _{exp}	Counts	Synthesis yield (%)
1	S ₁	4.18	73	0.81	1.24	3.8	20	20	10	5613	85
2	S ₂	4.18	73	0.54	0.86	4.16	23	24	12	3744	91
3	S ₃	4.17	73	0.51	0.80	7.90	30	28	10	4543	88
4	S ₄	4.18	73	0.69	1.1	4.23	25	24	11	4563	88
5	S ₅	4.18	73	0.67	1.00	3.78	19	19	10	6319	80
6	S ₆	4.18	73	0.87	1.32	2.64	17	18	11	6336	82

Table 1. Synthesized nanocatalysts Rietveld analysis and unit cell parameters.

Entry	Sample	2θ	B (rad)	D (nm)	δ	ε	d _{Bragg} (Å)	d _{hkl} (Å)	ρ _x (g/cm ³)	SSA (cm ² /g)
1	S ₁	43.26	0.006	25	0.0017	1.41	2.08	2.09	6.2	35
2	S ₂	43.25	0.007	22	0.0021	1.60	2.08	2.09	6.2	40
3	S ₃	43.31	0.007	21	0.0023	1.66	2.08	2.09	6.2	42
4	S ₄	43.26	0.006	24	0.0017	1.44	2.08	2.09	6.2	40
5	S ₅	43.28	0.006	25	0.0016	1.36	2.08	2.09	6.2	35
6	S ₆	43.26	0.005	30	0.0011	1.15	2.08	2.09	6.2	32

Table 2. Crystallite size (D), dislocation density (δ), strain data (ε), interplanar spacing (d) and X-ray density (ρ_x) of the as-synthesized nanomaterials.

According to Table 2, crystallite size changes by surfactant type. In this respect, the smallest and the largest crystallite size values are obtained when Hibiscus tea and Barberrry surfactants are used respectively.

The d values calculated by Bragg equation and Eq. (2) are in high consistency.

$$\frac{1}{d^2} = \left(\frac{h^2 + k^2 + l^2}{a^2} \right) \quad (2)$$

The dislocation parameter is a defect in a crystal related to the lattice improper resigstration of crystals from one part to another part. Hence, the defects in crystal system can be found using this parameter. The dislocation density δ [(lines/m²)10¹⁴] is calculated by the crystallite size (D) values with Eq. (3):

$$\delta = \frac{1}{D^2} \quad (3)$$

Change in dislocation density by varying the surfactant type was deduced. However, the change is not considerable. The highest and lowest δ values were obtained when Hibiscus tea (S₃) and Barberrry (S₆) surfactants were used respectively.

The parameter strain ε (10⁻³) value was determined with Eq. (4):

$$\varepsilon = \frac{\beta_{hkl} \cos \theta}{4} \quad (4)$$

According to Table 2, increase in the strain value with changing the surfactant type ion is probably because of the change in the crystallite degree. The smallest ε value is obtained when Barberrry (S₆) is used.

The parameter X-ray density (ρ_x) can be calculated by the following equation (Table 2):

$$\rho_x = \frac{ZM}{Na^3} \quad (5)$$

where M is the molecular weight of NiO (MW = 74.7 gmol⁻¹), N is the Avogadro number, Z is the number of formula unit per unit cell for NiO (Z = 4) and a is lattice parameter. As it is observed from ρ_x data, it is found that the X-ray density value is low and its variation by surfactant change is not notable. It can be concluded that no considerable change is occurred due to the impurity intercalation (with different density and atomic weight), when surfactant type is changed.

The specific surface area (SSA) per unit volume is a characteristic that can affect physical properties, chemical reactivity and photochemical efficiency. SSA can be calculated by measuring XRD density (ρ_{xrd}) and mean particle size (D) according to the Eq. (6):

$$SSA = \frac{6000}{D\rho_{xrd}} \quad (6)$$

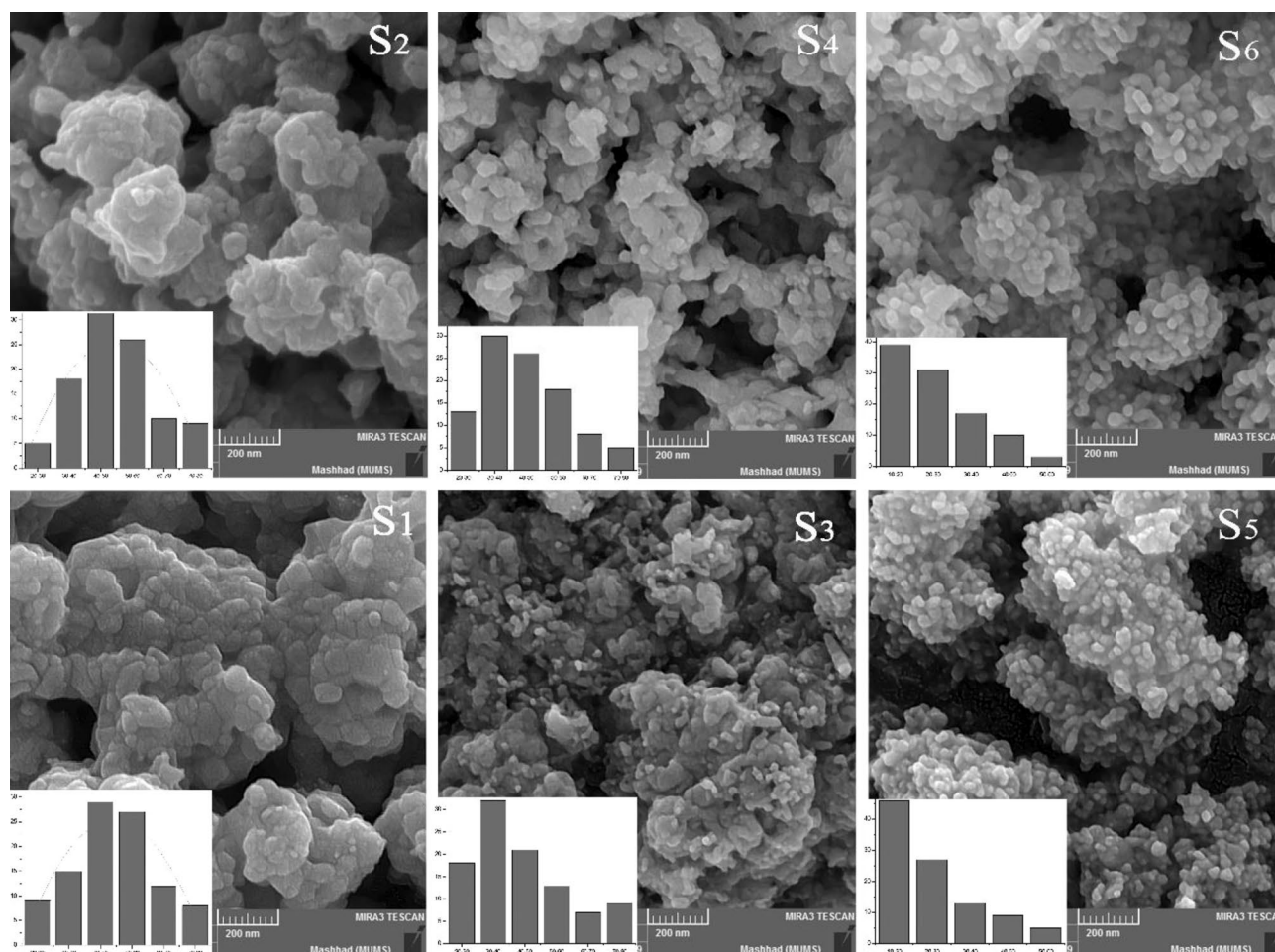


Figure 4. Effect of natural essence type on the morphology and the particle size distribution of synthesized NiO nanomaterials.

Morphology analysis. Figure 4 shows the FE-SEM images of the as-synthesized NiO nanomaterials. The insets are the particle size distribution calculated by software. The X and Y-axes are particle size (nm) and counts (%), respectively. As can be seen, the nanomaterials have porous morphology. It is clear that the final structure is formed by joining individual particles to each other. Besides, the size homogeneity and morphology of the particles are changed by surfactant type. In addition, no considerable homogeneity is observed for S_1 to S_3 but when Green tea (S_4), Rosemary (S_5) and Barberry (S_6) are used, the homogeneity is enhanced while the particle size is decreased. It was observed that the particle sizes were about 40–60, 40–60, 30–40, 30–40, 20–30 and 20–30 nm, for S_1 – S_6 , respectively.

Optical properties. The physical properties of the as-synthesized nanomaterials were investigated by studying the absorption spectra and direct optical band gap energies and investigating the essence type effect on the parameters.

The UV–Vis are shown in Fig. 5a and b. According to the results of Pascual et al.³¹ $(ah\nu)^n = A(h\nu - E_g)$ is the relation between the absorption coefficient and incident photon energy, where A is constant and E_g is the direct band gap energy if $n=2$. With extrapolating the linear part of the curve to the energy axis, the value of the direct band gap energies was evaluated. The E_g values were 2.45, 2.70, 2.30, 2.65, 2.65, and 2.50 eV, for S_1 – S_6 , respectively^{34–36}. The data indicate that the essence type can affect the E_g that may be due to the effect on the crystallite size of the as-synthesized nanomaterials.

FT-IR spectroscopy. According to the FTIR spectra (Fig. 6), the absorption peaks are observed at 401–420, 617, 1018, 1620 and 3800 cm^{-1} . The strong band at 401–420 and 617 cm^{-1} correspond to vibrations of Ni–O bonds^{36,37}. The band at 1018 cm^{-1} is assigned to C–O stretching vibration that can be associated to the residual extract compounds³⁶. The band at 1620 cm^{-1} can be attributed to the bending vibrations of water molecules. The peak at 3800 cm^{-1} is due to the O–H stretching vibrations^{45,46}.

Biginelli catalytic process. *Achieving optimal conditions by response surface methodology.* Several experimental designs can be used to find out the optimum level of factors in different reactions such as cata-

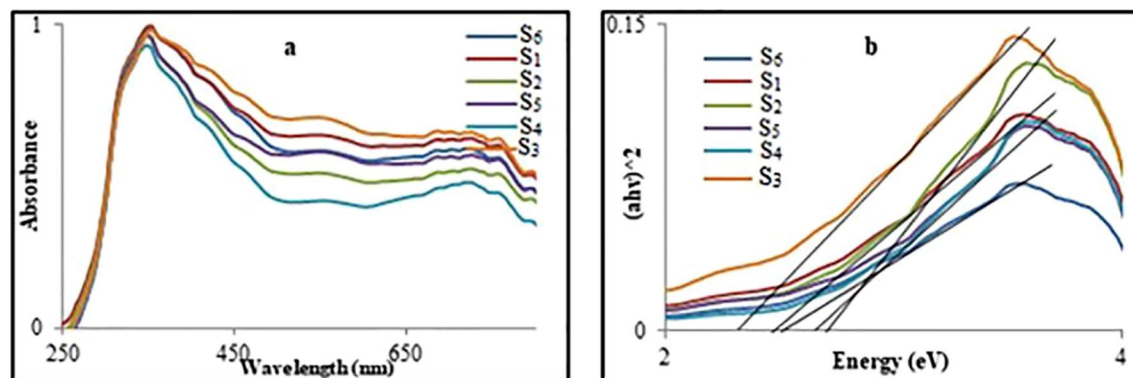


Figure 5. UV-Vis spectra (a) and NiO nanocatalyst band gap energy (b).

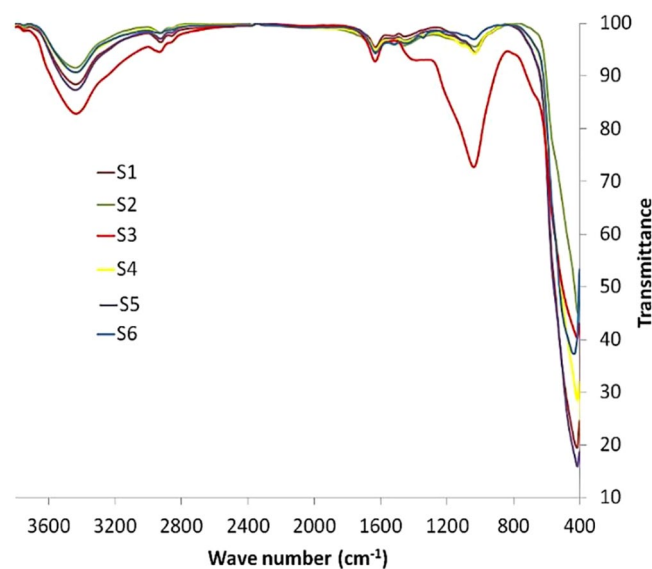


Figure 6. FTIR spectra of the prepared nanomaterials.

lytic processes. Full factorial design is one of the most interested experiment designs that combine all possible combination of the factors and their settings. Response surface methodology (RSM) is one of the methods that analyzes the experimental design by mathematical and statistical method using an empirical model and to evaluate the model, analysis of variance (ANOVA) was used. A proper analysis of variance requires some repeated experiments⁵⁰. In the present Biginelli reaction study, determination of the nanocatalyst amount, temperature and time was investigated and the outcome response is the yield (%). Various experiment designs of the aforementioned factors are tabulated in Table 3. The high and low factor levels are coded as (+ 1) and (− 1) respectively (Table 4). Four replicates at the center of the factors are considered for the validation of the model by ANOVA (Table 5). The factorial design data are fitted to a linear response model. Reaction yield (Y%) correlation with factors based on first order model is presented in Eq. (7):

$$Y\% = 60.80 + 15.63 \times A + 3.67 \times B + 5.05 \times C + 2.00 \times A \times B + 2.75 \times A \times C + 2.27 \times B^2 + 2.27 \times C^2 \quad (7)$$

The influence of each parameter on the reaction yield is shown by its coefficient in the equation. The more the value means higher effect. It can be seen that the catalyst is more effective than the other factors, in addition, the effect of temperature and time are close to each other.

Table 4, actual and coded forms of the designed experiments. The variables [amount of catalyst (A), temperature (B) and time (C)] are given in coded form (− α, − 1, 0, + 1, + α).

Investigation of the optimum conditions for the present Biginelli reactions was studied by ANOVA (Table 5) and the differences between group means were compared. This ratio of F-distribution (F-value) is the difference between group means. According to Table 5, the p-value of the regression was > 0.05 indicating that the model was significant at a high confidence level (95%)⁵⁰. Lack-of-fit test was used to confirm the adequacy of the fitted model. At 95% confidence level, the p-values for the lack-of-fits are < 0.05, which is not significant. Furthermore, ANOVA results strongly support the aforementioned discussion. In addition, the regression square (R²), adjusted

Entry	Catalyst (mg)	Temperature (°C)	Time (min)	Yield (%)
1	30	60	90	49
2	60	60	60	69
3	45	75	75	62
4	60	90	90	94
5	45	75	75	61
6	45	75	75	61
7	45	100	75	73
8	30	90	90	53
9	45	75	75	62
10	30	60	60	47
11	45	75	75	60
12	45	50	75	61
13	60	60	90	82
14	45	75	75	60
15	45	75	100	78
16	20	75	75	34
17	30	90	60	50
18	70	75	75	86
19	60	90	60	80
20	45	75	50	56

Table 3. Three-level full factorial design. Benzaldehyde, ethyl acetoacetate and urea (molar ratio: 1:1:1.2).

Entry	Factor	Name	Units	Low actual	High actual	Low coded	High coded	Mean	Std. dev.
1	A	Catalyst	Numeric	30.00	60.00	- 1.000	1.000	45.000	12.395
2	B	Temperature	Numeric	60.00	90.00	- 1.000	1.000	75.000	12.395
3	C	Time	Numeric	60.00	90.00	- 1.000	1.000	75.000	12.395

Table 4. Actual and coded forms of the designed experiments with the factors in CCD.

Entry	Source	Sum of squares	df	Mean square	F value	p-value prob > F	
1	Model	4099.6	7	585.66	249.23	< 0.0001	Significant
2	A	3336.22	1	3336.22	1419.76	< 0.0001	
3	B	184.39	1	184.39	78.47	< 0.0001	
4	C	348.61	1	348.61	148.35	< 0.0001	
5	AB	32	1	32	13.62	0.0031	
6	AC	60.5	1	60.5	25.75	0.0003	
7	B ²	75.17	1	75.17	31.99	0.0001	
8	C ²	75.17	1	75.17	31.99	0.0001	
9	Residual	28.2	12	2.35			
10	Lack of fit	24.2	7	3.46	4.32	0.0632	Not significant
11	Pure error	4	5	0.8			
12	Cor. total	4127.8	19				

Table 5. ANOVA output data for suggested first-order model.

(R²-adj) and predicted (R²-prd) regression values were applied to study the fitting quality of the linear model equation. It is evident that the R² = 0.99 for the variation fitting indicates high correlation of the response and the independent factors. Besides, high R²-adj = 0.98 and R²-prd = 0.97 reveals great relevance of the suggested model.

Optimum conditions for DHPMs synthesis were found with RSM. Figures S1 and S2 presented in the supplementary file shows the 2D and 3D plots, dispersal residuals and predicted values versus the experimental production efficiency data, respectively. The data revealed that the optimum condensation conditions of reaction were 60 mg of catalyst, 90 °C and 90 min reaction temperature and time respectively. Investigating the reaction kinetic of the present Biginelli reactions is important part to investigate the effect of parameters on the reaction

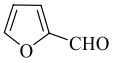
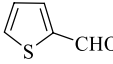
Entry	Ar	R	Yield ^a (%) S ₁	Yield ^a (%) S ₆	m.p. ^b (°C) S ₁	
					Obsd	Lit
1	C ₆ H ₅ CHO	EtO	94	97	201–203	202–203 ⁵¹
2	4-BrC ₆ H ₄ CHO	EtO	91	94	212–214	213–215 ⁵²
3	2-ClC ₆ H ₄ CHO	EtO	77	91	216–218	216–219 ⁵²
4	4-ClC ₆ H ₄ CHO	EtO	90	93	210–212	213–215 ⁵²
5	4-MeC ₆ H ₄ CHO	EtO	91	92	213–215	214–216 ⁵³
6	4-MeOC ₆ H ₄ CHO	EtO	75	79	201–203	201–202 ⁵²
7	4-O ₂ NC ₆ H ₄ CHO	EtO	53	61	206–210	207–208 ⁵²
8	2-HOC ₆ H ₄ CHO	EtO	74	78	213–214	214–215 ⁵⁴
9	4-HOC ₆ H ₄ CHO	EtO	86	86	233–235	232–234 ⁵⁵
10	C ₆ H ₅ CHO	MeO	92	93	203–205	206–209 ⁵³
11	4-BrC ₆ H ₄ CHO	MeO	84	87	241–243	240–242 ⁵²
12	2-ClC ₆ H ₄ CHO	MeO	78	86	228–230	226–229 ⁵⁶
13	4-ClC ₆ H ₄ CHO	MeO	89	91	202–205	204–207 ⁵²
14	4-MeC ₆ H ₄ CHO	MeO	90	91	201–203	202–204 ⁵³
15	4-MeOC ₆ H ₄ CHO	MeO	75	77	189–191	190–193 ⁵³
16	4-O ₂ NC ₆ H ₄ CHO	MeO	69	72	232–234	233–236 ⁵³
17	2-HOC ₆ H ₄ CHO	MeO	67	74	264–267	265–268 ⁵⁴
18	4-HOC ₆ H ₄ CHO	MeO	90	91	240–243	241–242 ⁵¹
19		EtO	92	93	207–210	209–210 ⁵⁷
20		EtO	90	91	214–216	215–217 ⁵⁷

Table 6. Catalytic performance of S₁ and S₆ at optimum conditions. ^aYield refers to isolated pure products. ^bProducts were characterized by comparison of melting points with the known products reported in the literature.

Entry	Sample	Ar	R	Product (mmol)	TON	TOF
1	S ₁	C ₆ H ₅ CHO	EtO	0.94	1.175	0.002285
2	S ₁	C ₆ H ₅ CHO	MeO	0.92	1.15	0.002236
3	S ₆	C ₆ H ₅ CHO	EtO	0.97	1.2125	0.002358
4	S ₆	C ₆ H ₅ CHO	MeO	0.93	1.1625	0.00226

Table 7. S₁ and S₆ catalytic performance comparison.

rate. The graphs in Fig. S2, exhibit a linear dependence at 0–90 min following a first-order kinetic model for the two samples. The equations and the reaction time plot for kinetic investigations are presented in Eqs. S1, S2 and Fig. S3 of supporting information.

Table 6, presents the catalytic activity data of S₁ and S₆ at the optimum condition. The purity of the as-prepared DHPMs compounds is investigated by measuring the melting points of the recrystallized DHPMs. The yield data indicate that S₆ catalytic activity is better than S₁ in almost all of the reactions. This can be due to the higher crystallinity (counts value), smaller particle size and higher surface area of S₆ than S₁.

The turnover numbers (TON, moles of product per mole of catalyst) for the synthesis of DHPMs were calculated by the following equation⁵⁸. The mmol amount of NiO was 0.8 at the optimized conditions.

$$\text{Turnover Number (TON)} = \frac{\text{mmol of product}}{\text{mmol of catalyst}} \quad (8)$$

Turnover frequency is obtained by the below relationship⁵⁹. $t_{1/2}$ is 360 min (4 run) and $\ln 2 = 0.7$.

$$\text{Turnover Frequency (TOF)} = \frac{0.7 \text{ TON}}{t_{1/2}} \quad (9)$$

S₁ and S₆ catalytic efficiency (Y%) comparison is presented in Table 7. It can be seen that the S₆ catalytic activity is better than S₁. In addition, the considerable yields were achieved when benzaldehyde, ethyl acetate and urea were used as raw materials.

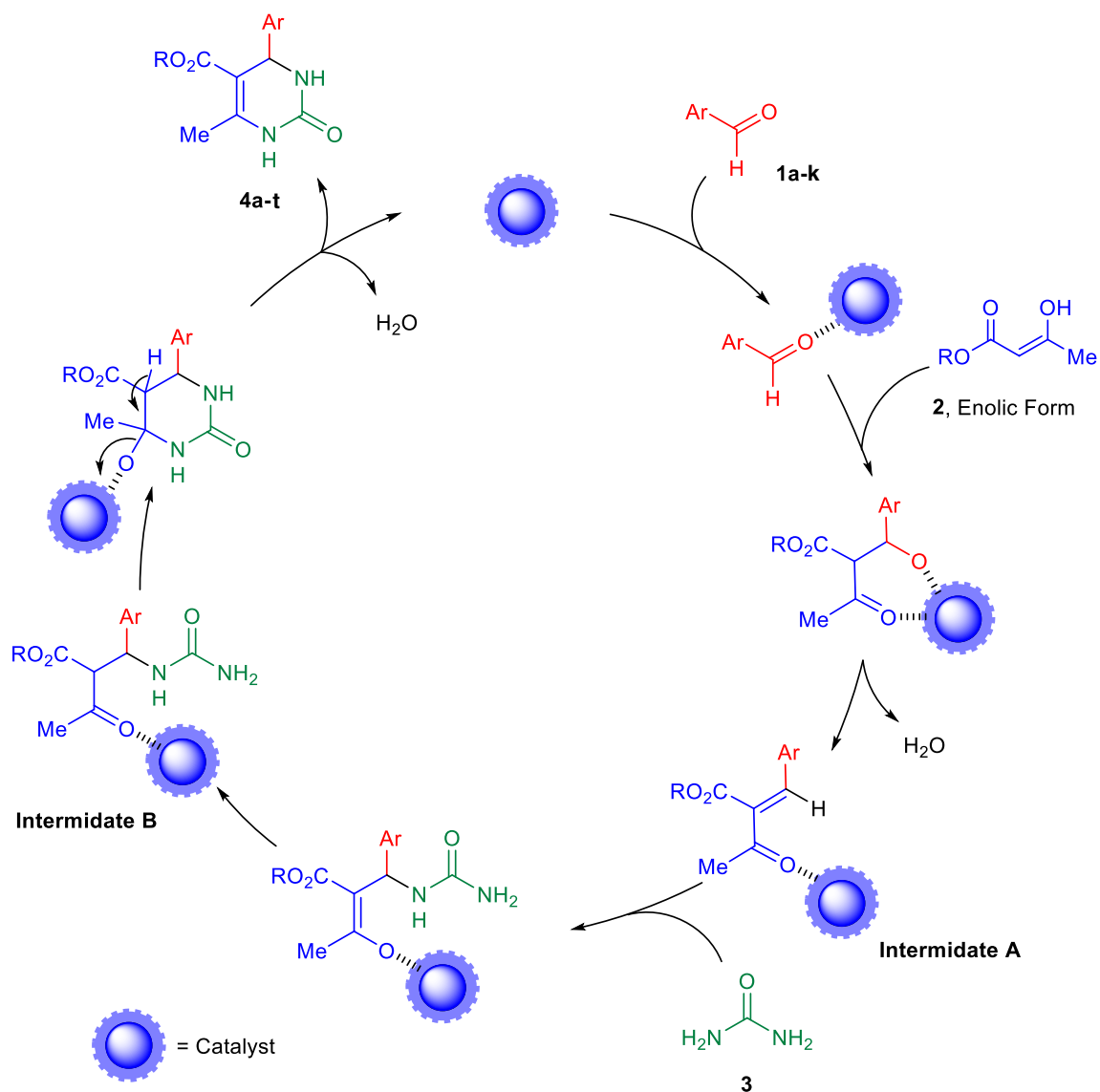


Figure 7. Proposed mechanistic route of MCRs Biginelli reaction catalyzed by NiO nanoparticles for the DHPMs synthesis.

The proposed reaction mechanism of the target products formation using NiO nanoparticles as catalyst is presented in Fig. 7.

In the initial step of reaction, the carbonyl groups of arylaldehydes **1a–k** and enolization of β -ketoester **2**, activated with nanoparticles occurs, afterwards, the *Knoevenagel* condensation between arylaldehydes **1a–k** with β -ketoester in enol-tautomeric forms to give the corresponding product as an intermediate α,β -unsaturated ketones **A** via dehydration.

In the next step, the *Michael* type addition of activated urea (**3**) molecules to the intermediate **A**, leads to the generation of open-chain ureide intermediate **B**, which, subsequently undergoes intramolecular cyclization of intermediate **B**, via elimination of H_2O molecule to afford the six membered heterocyclic compounds as the target DHPMs **4a–t**. In the present work, it is worthwhile to mention the crucial role of NiO as a catalyst under solvent-free conditions in the remarkable accelerating of all reaction stages. The NiO nanoparticle facilitates the formation of target products through Lewis acid sites (Ni^{2+}) coordinated to the oxygen of carbonyl groups. On the other hand, deprotonation of the C–H bond occurs in the presence of Lewis basic sites (O^{2-}). As a result, the formation of DHPM derivatives proceeds by activation of reactants through both Lewis acids and basic sites of NiO nanoparticles.

In order to study the effect of a parameter on the Biginelli reaction yield, the synthesized catalysts activity is scrutinized in Fig. 8a–f. In the present study, when a parameter is changed (for example time), the other two parameters maintain at the optimum values (for example temperature and catalyst) (Fig. 8a–c). According to the data, the optimum values are 60 mg catalyst, 90 °C temperature and 90 min time in which the catalytic reaction yield is 97%. The experiments shown in Fig. 8d–f, are conducted at the optimized reaction conditions. The data reveal that increasing each parameter has a positive influence on the catalytic efficiency of the as-synthesized

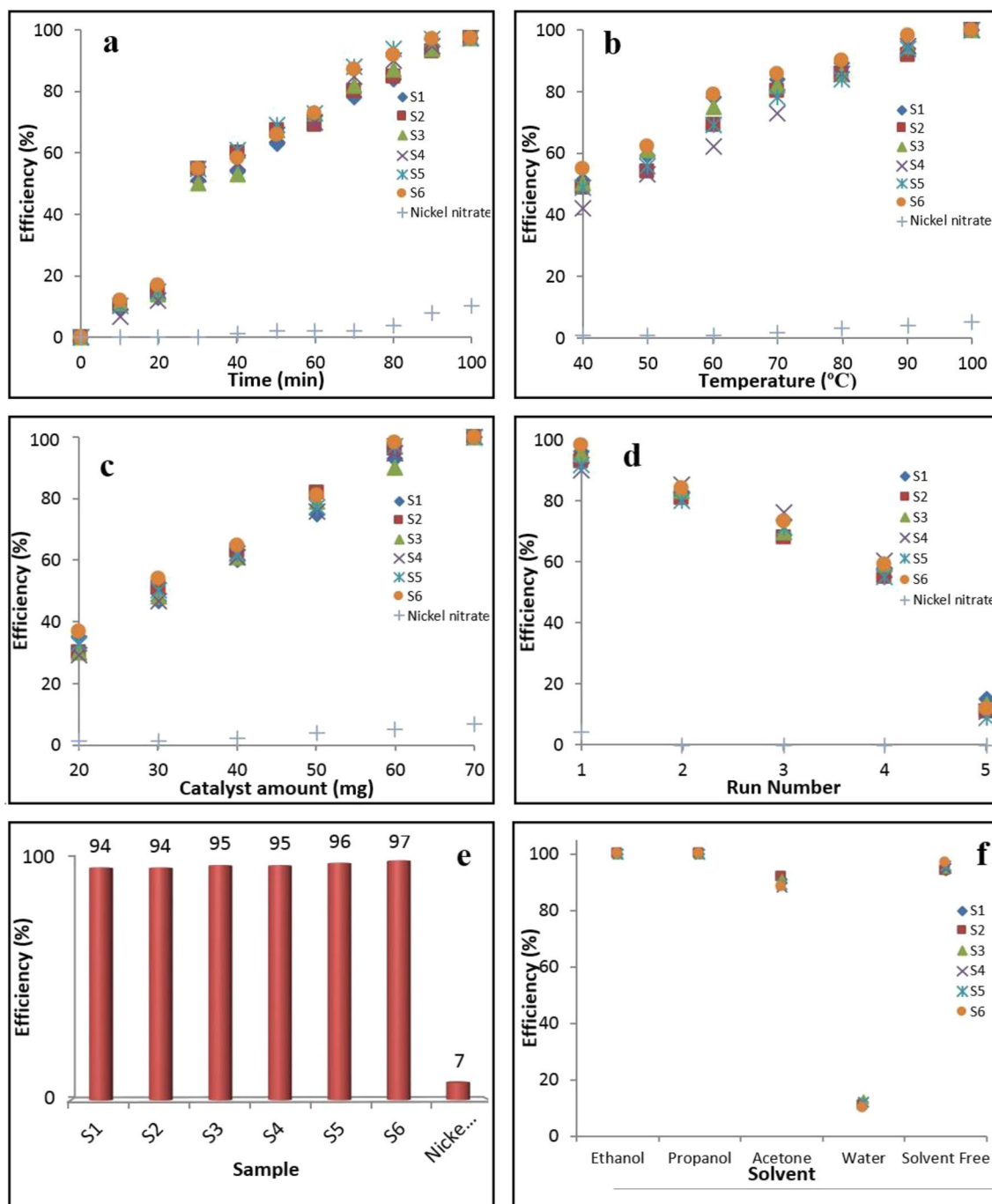


Figure 8. Effects of reaction time (a), temperature (b), catalyst amount (c), reusability (d), synthesized and raw material samples (e), and solvent type on the Biginelli catalytic efficiency (f). The experiments presented in (d–f), were done at the optimized conditions. The other experiments shown in the Figure done with the two factors at the optimized conditions.

samples. In addition, the influence of reaction time and temperature are more than catalyst amount effect on the reaction yield. Figure 8d, reveals that the recyclability of all of the catalysts is up to run 4. As it can be seen from the Fig. 8e, it is clear that S₆ keeps its activity longer than S₁ in the same reaction conditions. Figure 8f, shows that the organic solvents added to the reaction mixture play a medium and solve the raw materials until the contact surface is increased and the efficiency is enhanced. However, when H₂O was used as the solvent in the reaction mixture, it seems that it acts as an inhibitor and the reaction is not accomplished properly.

Figure 9 presents the XRD pattern of NiO nanocatalyst after 4 cycles of catalytic reaction. As can be found from the pattern, it is clear that the counts value of the sample decreases considerably. However, the nature of NiO is still maintained unchanged.

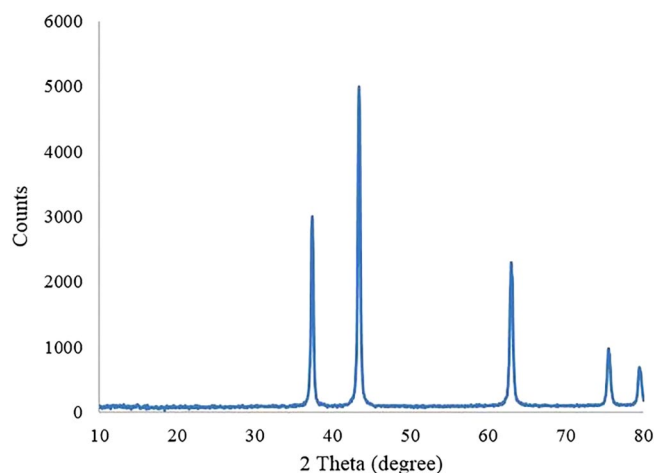


Figure 9. XRD pattern of S_5 after 4 runs catalytic reaction.

Entry	Catalyst	Ar	Catalyst amount	Reaction condition	Yield (%)	Time (min)	Ref.
1	$Zn(CH_3SO_3)_2 \cdot 4H_2O$	C_6H_5CHO	3 mmol	Ethanol, reflux	64	7 h	⁶⁰
2	CuI	C_6H_5CHO	15 mol%	Solvent-free, 90 °C	85	60	⁶¹
		4-Cl C_6H_4CHO			84	90	
3	$ZrO_2-Al_2O_3-Fe_3O_4$	C_6H_5CHO	50 mg	Ethanol, reflux, 140 °C	82	300	⁶²
		2-Cl C_6H_4CHO			40		
		4-Cl C_6H_4CHO			66		
4	ZnO	C_6H_5CHO	25 mol%	Solvent-free, 90 °C	92	50	⁶³
		4-Cl C_6H_4CHO			95		
5	$SbCl_5 \cdot SiO_2$	C_6H_5CHO	100 mg	Solvent-free, room temperature	95	12	⁶⁴
		4-Cl C_6H_4CHO			93	20	
6	PANI- $FeCl_3$	C_6H_5CHO	0.24 mmol	CH_3CN , reflux	83	24 h	⁶⁵
		2-Cl C_6H_4CHO			84		
		4-Cl C_6H_4CHO			90		
7	Sm^{3+} -Doped $Bi_2Mn_2O_7$	C_6H_5CHO	14 mg	Solvent-free, 104 °C	82	66	⁶⁶
		2-Cl C_6H_4CHO			71		
		4-Cl C_6H_4CHO			37		
8	S_1	C_6H_5CHO	60 mg	Solvent-free, 90 °C	94	90	This work
		2-Cl C_6H_4CHO			77		
		4-Cl C_6H_4CHO			90		
9	S_6	C_6H_5CHO	60 mg	Solvent-free, 90 °C	97	90	This work
		2-Cl C_6H_4CHO			91		
		4-Cl C_6H_4CHO			93		

Table 8. Comparison of synthesized NiO nanocatalyst with other catalysts.

A comparison of S_1 and S_6 catalysts with other previously reported catalysts for the synthesis of DHPMs using the H, 2-Cl and 4-Cl derivatives is tabulated in Table 8 that confirm the competency of this research. The most important factors affecting the reaction outcome: catalytic reaction, the catalyst amount, reaction time and temperature comparison with other reported researches affirms the excellence of current work. According to the data, some higher efficiencies are achieved only when the reaction duration and temperature were higher than the present research. Furthermore, composite materials⁵⁹⁻⁶⁵ have decreased yield in compare of other studies.

Conclusion

This research aimed to report a systematic study of the surfactant type influence on the physical properties of the as-fabricated NiO nanomaterials and using the materials as low cost and toxicity and high efficient recyclable catalysts for the synthesis of DHPMs. NiO nanomaterials were synthesized with a green procedure. The Rietveld analysis data revealed that the surfactant type changed the crystallographic parameters. It was found that the lowest and highest crystal phase growth was achieved when Yarrow and Barberry surfactants were

used, respectively. FE-SEM images revealed a change in the morphology from non-homogeneous to homogeneous spherical particles after change in surfactant type from orange blossom to barberryas. DHPMs optimum synthesis conditions were catalyst: 60 mg, reaction temperature: 90 °C and reaction time: 90 min. The purity of the DHPMs was investigated by recrystallizing and measuring the melting points. The yield at the optimized conditions was 94% and 97% for S_1 and S_6 , respectively. Langmuir–Hinshelwood (L–H) kinetic model affirmed the pseudo-first order kinetic model of present Biginelli reactions. The K_{app} values confirmed the faster reaction using S_6 in compare to S_1 . Better catalytic efficacy was obtained for S_6 .

Data availability

All data generated or analyzed during this study are included in this published article [and its supplementary information files].

Received: 27 January 2022; Accepted: 12 May 2022

Published online: 20 May 2022

References

- Zinicovscaia, I. Use of bacteria and microalgae in synthesis of nanoparticles. *Chem. J. Mold.* **2**, 32–38 (2012).
- Chrissanthopoulos, A. *et al.* Synthesis and characterization of ZnO/NiO p–n heterojunctions: ZnO nanorods grown on NiO thin film by thermal evaporation. *Photon. Nanostruct. Fundam. Appl.* **9**, 132–139 (2011).
- Derikvand, Z., Rahmati, F. & Azadbakht, A. Nano NiO/AlMCM-41, a green synergistic, highly efficient and recyclable catalyst for the reduction of nitrophenols. *Appl. Organomet. Chem.* **33**, e4864 (2019).
- Iqbal, J. *et al.* Green synthesis and characterizations of Nickel oxide nanoparticles using leaf extract of *Rhamnus virgata* and their potential biological applications. *Appl. Organomet. Chem.* **33**, e4950 (2019).
- Wang, X. *et al.* Optical and electrochemical properties of nanosized NiO via thermal decomposition of nickel oxalate nanofibres. *Nanotechnol.* **16**, 37–39 (2005).
- Bahari Molla Mahaleh, Y., Sadrnezhaad, S. K. & Hosseini, D. NiO nanoparticles synthesis by chemical precipitation and effect of applied surfactant on distribution of particle size. *J. Nanomater.* **2008**, 470595 (2008).
- Nathan, T., Aziz, A., Noor, A. F. & Prabaharan, S. R. S. Nanostructured NiO for electrochemical capacitors: synthesis and electrochemical properties. *J. Solid State Electrochem.* **12**, 1003–1009 (2008).
- Ganachari, S. V., Bhat, R., Deshpande, R. & Venkataraman, A. Synthesis and characterization of nickel oxide nanoparticles by self-propagating low temperature combustion method. *Rec. Res. Sci. Technol.* **4**, 50–53 (2012).
- Mahdavi, B., Paydarfard, S., Rezaei-Seresht, E., Baghayeri, M. & Nodehi, M. Green synthesis of NiONPs using *Trigonella subenervis* extract and its applications as a highly efficient electrochemical sensor, catalyst, and antibacterial agent. *Appl. Organomet. Chem.* **35**, e6264 (2021).
- Buazar, F., Alipouryan, S., Kroushawi, F. & Hossieni, S. A. Photodegradation of odorous 2-mercaptobenzoxazole through zinc oxide/hydroxyapatite nanocomposite. *Appl. Nanosci.* **5**, 719–729 (2015).
- Ezhilarasi, A. A. *et al.* Green synthesis of NiO nanoparticles using *Aegle marmelos* leaf extract for the evaluation of in-vitro cytotoxicity, antibacterial and photocatalytic properties. *J. Photochem. Photobiol. B.* **180**, 39–50 (2018).
- Ezhilarasi, A. *et al.* Green synthesis of NiO nanoparticles using *Moringa oleifera* extract and their biomedical applications: Cytotoxicity effect of nanoparticles against HT-29 cancer cells. *J. Photochem. Photobiol. B.* **164**, 352–360 (2016).
- Xiang, L., Deng, X. Y. & Jing, Y. Experimental study on synthesis of NiO nanoparticles. *Scr. Mater.* **47**, 219–224 (2002).
- Hosny, N. M. Synthesis, characterization and optical band gap of NiO nanoparticles derived from anthranilic acid precursors via a thermal decomposition route. *Polyhedron* **30**, 470–476 (2011).
- Li, X., Zhang, X., Li, Z. & Qian, Y. Synthesis and characteristics of NiO nanoparticles by thermal decomposition of nickel dimethylglyoximate rods. *Solid State Commun.* **137**, 581–584 (2006).
- Wang, Y. & Ke, J. J. Preparation of nickel oxide powder by decomposition of basic nickel carbonate in microwave field with nickel oxide seed as a microwave absorbing additive. *Mater. Res. Bull.* **31**, 55–61 (1996).
- Pulimi, V. R. R. & Jeevanandam, P. The effect of anion on the magnetic properties of nanocrystalline NiO synthesized by homogeneous precipitation. *J. Magn. Mater.* **321**, 2556–2562 (2009).
- Anandan, K. & Rajendran, V. Morphological and size effects of NiO nanoparticles via solvothermal process and their optical properties. *Solid State Electron.* **14**, 43–47 (2011).
- Wei, Z., Qiao, H., Yang, H., Zhang, C. & Yan, X. Characterization of NiO nanoparticles by anodic arc plasma method. *J. Alloys Compd.* **479**, 855–858 (2009).
- Mohseni Meybodi, S., Hosseini, S. A., Rezaee, M., Sadrnezhaad, S. K. & Mohammadyani, D. Synthesis of wide band gap nanocrystalline NiO powder via a sonochemical method. *Ultrason. Sonochem.* **19**, 841–845 (2012).
- Du, Y. *et al.* Preparation of NiO nanoparticles in microemulsion and its gas sensing performance. *Mater. Lett.* **68**, 168–170 (2012).
- Wang, X. *et al.* High-yield synthesis of NiO nanoplatelets and their excellent electrochemical performance. *Cryst. Growth Des.* **6**, 2163–2165 (2006).
- Nasseri, M. A., Ahrari, F. & Zakerinasab, B. A green biosynthesis of NiO nanoparticles using aqueous extract of *Tamarix serotina* and their characterization and application. *Appl. Organomet. Chem.* **30**, 978–984 (2016).
- Moharekar, S., Raskar, P. & Wani, A. Synthesis and comparative study of zinc oxide nanoparticles with and without capping of pectin and its application. *World. J. Pharm. Pharm. Sci.* **37**, 1255–1267 (2014).
- Buazar, F. *et al.* Potato extract as reducing agent and stabiliser in a facile green one-step synthesis of ZnO nanoparticles. *J. Exp. Nanosci.* **11**, 175–184 (2016).
- Khalafi, T., Buazar, F. & Ghanemi, K. Phycosynthesis and enhanced photocatalytic activity of Zinc oxide nanoparticles toward organosulfur pollutants. *Sci. Rep.* **9**, 6866 (2019).
- Sepahvand, M., Buazar, F. & Sayahi, M. H. Novel marine-based gold nanocatalyst in solvent-free synthesis of polyhydroquinoline derivatives: Green and sustainable protocol. *Appl. Organomet. Chem.* **34**, e6000 (2020).
- Moavi, J., Buazar, F. & Sayahi, M. H. Algal magnetic nickel oxide nanocatalyst in accelerated synthesis of pyridopyrimidine derivatives. *Sci. Rep.* **11**, 6296 (2021).
- Safat, S., Buazar, F., Albukhaty, S. & Matroodi, S. Enhanced sunlight photocatalytic activity and biosafety of marine-driven synthesized cerium oxide nanoparticles. *Sci. Rep.* **11**, 14734 (2021).
- Azimi, F., Poursattar Marjani, A. & Keshipour, S. Fe(II)-phthalocyanine supported on chitosan aerogel as a catalyst for oxidation of alcohols and alkyl arenes. *Sci. Rep.* **11**, 23769 (2021).
- Pascual, J., Camassel, J. & Mathieu, M. Fine structure in the intrinsic absorption edge of TiO₂. *Phys. Rev. B.* **18**, 5606–5614 (1978).
- Tekin, V. *et al.* Green synthesis of silver nanoparticles by using eugenol and evaluation of antimicrobial potential. *Appl. Organomet. Chem.* **33**, e4969 (2019).

33. Iqbal, J. *et al.* Potential phytochemicals for developing breast cancer therapeutics: Nature's healing touch. *Eur. J. Pharmacol.* **827**, 125–148 (2018).
34. Singh, P., Kim, Y.-J., Zhang, D. & Yang, D.-C. Biological synthesis of nanoparticles from plants and microorganisms. *Trends Biotechnol.* **34**, 588–599 (2016).
35. Ahmed, S., Ahmad, M., Swami, B. L. & Ikram, S. A review on plants extract mediated synthesis of silver nanoparticles for antimicrobial applications: A green expertise. *J. Adv. Res.* **7**, 17–28 (2016).
36. Duran, N. & Seabra, A. B. Biogenic synthesized Ag/Au nanoparticles: Production, characterization, and applications. *Curr. Nanosci.* **14**, 82–94 (2018).
37. Iqbal, J. *et al.* Ursolic acid a promising candidate in the therapeutics of breast cancer: Current status and future implications. *Biomed. Pharmacother.* **108**, 752–756 (2018).
38. Buazar, F., Sweidi, S., Badri, M. & Kroushawi, F. Biofabrication of highly pure copper oxide nanoparticles using wheat seed extract and their catalytic activity: A mechanistic approach. *Green Process. Synth.* **8**, 691–702 (2019).
39. Zhang, M., Liu, Y.-H., Shang, Z.-R., Hu, H.-C. & Zhang, Z.-H. Supported molybdenum on graphene oxide/Fe₃O₄: An efficient, magnetically separable catalyst for one-pot construction of spiro-oxindole dihydropyridines in deep eutectic solvent under microwave irradiation. *Catal. Commun.* **88**, 39–44 (2017).
40. Chen, M.-N., Mo, L.-P., Cui, Z.-S. & Zhang, Z.-H. Magnetic nanocatalysts: Synthesis and application in multicomponent reactions. *Curr. Opin. Green Sustain. Chem.* **15**, 27–37 (2019).
41. Anvari Gharabaghlu, M., Shadjou, N. & Poursattar Marjani, A. Cu@KCC-1-NH-CS₂ as a new and highly efficient nanocatalyst for the synthesis of 2-amino-4H-chromene derivatives. *Appl. Organomet. Chem.* **34**, e5868 (2020).
42. Majidi Arlan, F., Poursattar Marjani, A., Javahershenas, R. & Khalafy, J. Recent developments in the synthesis of polysubstituted pyridines via multicomponent reactions using nanocatalysts. *New J. Chem.* **45**, 12328–12345 (2021).
43. Kalidhar, S. B. & Sharma, P. Physcion-8-O-gentiobioside from *Rhamnus virgata*. *Phytochemistry* **23**, 1196–1197 (1984).
44. Karimi-Jaberi, Z. & Moaddeli, M. S. Synthesis of 3,4-dihydropyrimidin-2(1H)-ones and their corresponding 2(1H)thiones using trichloroacetic acid as a catalyst under solvent-free conditions. *ISRN Org. Chem.* **2012**, 474626 (2012).
45. Shahid, A. *et al.* Solvent-free Biginelli reactions catalyzed by hierarchical zeolite utilizing a ball mill technique: A green sustainable process. *Catalyst.* **7**, 84–101 (2017).
46. Gonçalves, I. L. *et al.* Versatility of the Biginelli reaction: Synthesis of new biphenyl dihydropyrimidin-2-thiones using different ketones as building blocks. *Tetrahedron Lett.* **59**, 2759–2762 (2018).
47. Gümüş, M. K., Gorobets, N. Y., Sedash, Y. V., Shishkina, S. V. & Desenko, S. M. Rapid formation of chemical complexity via a modified Biginelli reaction leading to dihydrofuran-2(3H)-one spiro-derivatives of triazol[1,5-a]pyrimidine. *Tetrahedron Lett.* **58**, 3446–3448 (2017).
48. Esmaili, R., Kafi-Ahmadi, L. & Khademinia, Sh. A highly efficient one-pot multicomponent synthesis of 3,4-dihydropyrimidin-2-(1H)-ones/thiones catalyzed by strontium pyroarsenate nano-plates. *J. Mol. Struct.* **1216**, 128124 (2020).
49. Kafi-Ahmadi, L., Poursattar Marjani, A. & Nozad, E. Ultrasonic-assisted preparation of Co₃O₄ and Eu-doped Co₃O₄ nanocatalysts and their application for solvent-free synthesis of 2-amino-4H-benzochromenes under microwave irradiation. *Appl. Organomet. Chem.* **35**, e6271 (2021).
50. Box, G. E. P. & Draper, N. R. *Empirical Model-Building and Response Surfaces* (Wiley, 1987).
51. Aswin, K., Mansoor, S. S., Logaiya, K., Sudhan, P. N. & Ahmed, R. N. Facile synthesis of 3,4-dihydropyrimidin-2(1H)-ones and -thiones and indeno[1,2-d]pyrimidines catalyzed by *p*-dodecylbenzenesulfonic acid. *J. Taibah Univ. Sci.* **8**, 236–247 (2014).
52. Borse, A., Patil, M., Patil, N. & Shinde, R. A green, expeditious, one-pot synthesis of 3,4-dihydropyrimidin-2(1H)-ones using a mixture of phosphorus pentoxide-methanesulfonic acid at ambient temperature. *ISRN Org. Chem.* **2012**, 415645 (2012).
53. Fan, X., Zhang, X. & Zhang, Y. Samarium chloride catalysed Biginelli reaction: One-pot synthesis of 3,4-dihydropyrimidin-2(1H)-ones. *J. Chem. Res.* **2002**, 436–438 (2002).
54. Diarjani, E. S., Rajabi, F., Yahyazadeh, A., Puente-Santiago, A. R. & Luque, R. Copper tridentate schiff base complex supported on SBA-15 as efficient nanocatalyst for three-component reactions under solventless conditions. *Materials.* **11**, 2458–2469 (2018).
55. Mohamadpour, F. Development of an environment-friendly and solvent-free synthetic route for the synthesis of 3,4-dihydropyrimidin-2-(1H)-ones/thiones using La(NO₃)₃·6H₂O as an efficient catalyst. *Makara J. Sci.* **22**, 142–148 (2018).
56. Xu, H. & Wang, Y.-G. One-pot construction 3,4-dihydropyrimidin-2(1H)-ones catalysed by samarium(III). *J. Chem. Res.* **2003**, 377–379 (2003).
57. Fu, N.-Y. *et al.* Indium(III) bromide-catalyzed preparation of dihydropyrimidinones: Improved protocol conditions for the Biginelli reaction. *Tetrahedron* **58**, 4801–4807 (2002).
58. Yamaguchi, K. & Mizuno, N. Supported ruthenium catalyst for the heterogeneous oxidation of alcohols with molecular oxygen. *Angew. Chem. Int. Ed.* **41**, 4538–4542 (2002).
59. Kozuch, S. & Martin, M. L. “Turning Over” definitions in catalytic cycles. *ACS Catal.* **2**, 2787–2794 (2012).
60. Wang, M., Jiang, H. & Wang, Z. Biginelli condensation of aliphatic aldehydes catalysed by zinc methanesulfonate. *J. Chem. Res.* **2005**, 691–693 (2005).
61. Kalita, H. R. & Phukan, P. CuI as reusable catalyst for the Biginelli reaction. *Catal. Commun.* **8**, 179–182 (2007).
62. Wang, A., Liu, X., Su, Z. & Jing, H. New magnetic nanocomposites of ZrO₂-Al₂O₃-Fe₃O₄ as green solid acid catalysts in organic reactions. *Catal. Sci. Technol.* **4**, 71–80 (2014).
63. Hassanpour, A., Abolhasani, J. & Hosseinzadeh Khanmiri, R. One-pot and green procedure for the synthesis of 3,4-dihydropyrimidin-2(1H)-(thio)ones using ZnO nanoparticles as a solid acid catalyst. *J. Korean Chem. Soc.* **58**, 445–449 (2014).
64. Bamoniri, A., Mirjalili, B. F. & Karbasizadeh, H. Nano SbCl₅·SiO₂: An efficient and heterogeneous catalyst for the synthesis of 3,4-dihydropyrimidin-2(1H)-one (thione)derivatives under solvent-free conditions. *Sci. Iran.* **22**, 2332–2340 (2015).
65. Patel, H. A., Sawant, A. M., Rao, V. J., Patel, A. L. & Bedekar, A. V. Polyaniline supported FeCl₃: An effective heterogeneous catalyst for Biginelli reaction. *Catal. Lett.* **147**, 2306–2312 (2017).
66. Khademinia, Sh. & Behzad, M. Hydrothermal synthesis, characterization and catalytic performance of La³⁺ and Sm³⁺: Doped Bi₂Mn₂O₇ nanocatalysts for Biginelli reactions. *J. Nanostruct.* **9**, 172–182 (2019).

Acknowledgements

The authors would like to acknowledge the support received from the Research Council of Urmia University.

Author contributions

M.K.: Data curation, investigation, methodology. L.K.-A.: Conceptualization, data curation, formal analysis, funding acquisition, investigation, methodology, project administration, resources, supervision, validation, visualization, writing-original draft, and writing-review & editing. S.K.: Conceptualization, data curation, formal analysis, investigation, methodology, supervision, and writing-review & editing. A.P.M.: Conceptualization, data curation, formal analysis, investigation, methodology, supervision, validation, visualization, and writing-review & editing. E.N.: Investigation, writing-review & editing.

Competing interests

The authors declare no competing interests.

Additional information

Supplementary Information The online version contains supplementary material available at <https://doi.org/10.1038/s41598-022-12589-4>.

Correspondence and requests for materials should be addressed to L.K.-A.

Reprints and permissions information is available at www.nature.com/reprints.

Publisher's note Springer Nature remains neutral with regard to jurisdictional claims in published maps and institutional affiliations.



Open Access This article is licensed under a Creative Commons Attribution 4.0 International License, which permits use, sharing, adaptation, distribution and reproduction in any medium or format, as long as you give appropriate credit to the original author(s) and the source, provide a link to the Creative Commons licence, and indicate if changes were made. The images or other third party material in this article are included in the article's Creative Commons licence, unless indicated otherwise in a credit line to the material. If material is not included in the article's Creative Commons licence and your intended use is not permitted by statutory regulation or exceeds the permitted use, you will need to obtain permission directly from the copyright holder. To view a copy of this licence, visit <http://creativecommons.org/licenses/by/4.0/>.

© The Author(s) 2022